A&A 475, 801–812 (2007)
DOI: 10.1051/0004-6361:20065217

Astronomy & Astrophysics

The 12 μm *ISO*-ESO-Sculptor* and 24 μm *Spitzer* faint counts reveal a population of ULIRGs as dusty massive ellipticals

Evolution by types and cosmic star formation

B. Rocca-Volmerange[1,2], V. de Lapparent[1], N. Seymour[1,3], and M. Fioc[1]

[1] Institut d'Astrophysique de Paris, UMR7095 CNRS, Université Pierre et Marie Curie – Paris 6, 98bis boulevard Arago, 75014 Paris, France
e-mail: brigitte.rocca@iap.fr
[2] Université Paris Sud, Bât 121, 91405 Orsay Cedex, France
[3] Spitzer Science Center, California Institute of Technology, Mail Code 220-6, 1200 East California Boulevard, Pasadena, CA 91125, USA

Received 16 March 2006 / Accepted 20 June 2007

ABSTRACT

Context. Multi-wavelength galaxy number counts provide clues to the nature of galaxy evolution. The interpretation per galaxy type of the mid-IR faint counts obtained with *ISO* and *Spitzer*, consistent with the analysis of deep UV-optical-near IR galaxy counts, provide new constraints on the dust and stellar emission. Discovering the nature of new populations, such as high redshift ultra-luminous ($\geq 10^{12}$ $L_\odot$) infrared galaxies (ULIRGs), is also crucial for understanding galaxy evolution at high redshifts.
Aims. We first present the faint galaxy counts at 12 μm from the catalogue of the *ISO*-ESO-Sculptor Survey (*ISO*-ESS) published in a companion article (Seymour et al. 2007a, A&A, 475, 791). They go down to 0.31 mJy after corrections for incompleteness. We verify the consistency with the existing *ISO* number counts at 15 μm. Then we analyse the 12 μm (*ISO*-ESS) and the 24 μm (*Spitzer*) faint counts, to constrain the nature of ULIRGs, the cosmic star formation history and time scales for mass buildup.
Methods. We show that the "normal" scenarios in our evolutionary code PÉGASE, which had previously fitted the deep UV-optical-near IR counts, are unsuccessful at 12 μm and 24 μm. We thus propose a new ULIRG scenario adjusted to the observed cumulative and differential 12 μm and 24 μm counts and based on observed 12 μm and 25 μm IRAS luminosity functions and evolutionary optical/mid-IR colours from PÉGASE.
Results. We succeed in simultaneously modelling the typical excess observed at 12 μm, 15 μm (*ISO*), and 24 μm (*Spitzer*) in the cumulative and differential counts by only changing 9% of normal galaxies (1/3 of the ellipticals) into ultra-bright dusty galaxies evolving as ellipticals, and interpreted as distant ULIRGs. These objects present similarities with the population of radio-galaxy hosts at high redshift. No number density evolution is included in our models even if minor starbursts due to galaxy interactions remain compatible with our results.
Conclusions. Higher spectral and spatial resolution in the mid-IR, together with submillimeter observations using the future *Herschel* observatory, will be useful to confirm these results.

Key words. infrared: galaxies – galaxies: evolution – galaxies: photometry – cosmology: observations

1. Introduction

The mid-infrared extra-galactic source counts provide clues on the evolution of galaxies at high z and allow us to follow the cosmic star formation history up to when the Universe was only one quarter of its present age. The high sensitivity of the infrared deep surveys observed with ESA's *Infrared Space Observatory ISO* (Kessler et al. 2003), and more recently with *Spitzer Space Telescope* (Werner et al. 2004), offers an unique opportunity to study the obscured star formation process through the emission of grains heated by young stars and possibly by an active nucleus, thus reaching galaxies at their earliest epochs. Interactions of galaxies are known to explain the huge IR emission detected in local Ultra Luminous Infra Red Galaxies (ULIRG; Soifer et al. 1984). One crucial issue is whether ULIRGs provide observational evidence that galaxy interactions play a fundamental role in galaxy evolution. Moreover, because the infrared luminosity depends on the dust mass accumulated from stellar ejecta, it provides complementary diagnostics of past star formation that may in turn be used to model the star formation history.

Over the years, a long series of deep surveys from the UV to the optical, down to the extreme depth of the Hubble Deep Field North (HDF-N) at $B = 29$ (Williams et al. 1996), have constrained the direct stellar emission in terms of cosmology and scenarios of star formation. Fioc & Rocca-Volmerange (1999a) derived a set of galaxy populations fitting the multi-wavelength (UV-optical-near infrared) deep galaxy counts dominated by stellar emission. This set defines the evolution scenarios of eight galaxy types and their number fractions. In the

* Based on observations with *ISO*, an ESA project with instruments funded by ESA member states (specially the PI countries France, Germany, The Netherlands, and the United Kingdom) with the participation of ISAS and NASA. The ESO-Sculptor Survey is based on observations collected at the European Southern Observatory (ESO), La Silla, Chile.

mid-infrared, galaxy light is dominated by the emission from dust grains in the form of graphite, silicates, or polycyclic aromatic hydrocarbons (PAH; Puget & Léger 1989). Because different time scales characterise the evolution of star and dust emissions, the results of optical and mid-infrared source counts may differ significantly.

Two difficulties however hamper the interpretation of data. One is the lack of homogeneity between the various surveys: due to large-scale galaxy clustering, the statistical properties derived from deep pencil-beam surveys suffer from "cosmic variance" (Somerville et al. 2004) and might thus differ from the analyses on large area surveys. Another difficulty is the variety of sources (starbursts due to mergers, normal evolved galaxies, AGNs) and their intrinsic evolution. As an example, the time scale of star formation associated to galaxy interactions is significantly shorter ($\simeq 10^8$ yrs) than the star formation time scales of galaxy populations ($>10^9$ yrs, depending on spectral type) observed in deep surveys. We consider the contribution of AGNs to be minimal at the flux density range explored here, but the impact of an embedded hidden AGN is discussed below.

Our large area *ISOCAM* ESO-Sculptor Survey (*ISO*-ESS) at 12 μm, published in the companion paper (Seymour et al. 2007a), here tackles these various limitations by covering a significant area and by using the new code PÉGASE.3 (Fioc et al. 2007) which coherently predicts the evolving stellar and grain emissions from evolved galaxies as well as young starbursts. It is able to predict *both* starlight and dust emission from the UV to the far infrared, by taking the transfer and the reprocessing of light in the different wavelength domains into account. A large variety of star formation time scales is considered in our evolutionary templates, but no evolution of the number density of galaxies is included in the model.

Several other major surveys in the mid-infrared have been performed with the *ISOCAM* camera, and they also provide deep galaxy counts. The largest survey is ELAIS (Rowan-Robinson et al. 1999, 2004), which covers 12 sq. deg. in the flux range 0.45–150 mJy at wavelengths of 6.7 μm (*LW2*) and 15 μm (*LW3*); the corresponding galaxy counts were published by Serjeant et al. (2000). Following the preliminary surveys of Taniguchi et al. (1997) and Oliver et al. (1997), several major surveys have also been performed that provide deep galaxy counts. Among them are the *ISO* 15 μm observations of the Lockman Deep Field, the Marano-ROSAT Ultra Deep Field (Aussel et al. 1999; Elbaz et al. 1999) and the Lockman Shallow Field (Flores et al. 1999). Even deeper surveys have been obtained in the *LW2* and *LW3* filters, centered on Abell cluster 2390 (Altieri et al. 1999), the HDF field, and other fields covering areas of 2.5 arcmin in radius (Oliver et al. 2000, 2002), and of 16 arcmin^2 (Sato et al. 2003). These various surveys yield galaxy number counts in reasonable agreement and detect an excess in the number of galaxies at faint fluxes (below ~1 mJy), which is often interpreted as an increase in the star formation rate with look-back time. For example, Pozzi et al. (2004) fit the 15 μm number counts by introducing a population of evolving starbursts, based on the local star-forming prototype M 82 (Silva et al. 1998), which undergoes very strong luminosity or density evolution parameterized as $(1+z)^{\alpha}$, with $\alpha \simeq 3-4$.

All the differential 24 μm counts also show a systematic departure from an Euclidean Universe at fluxes fainter than ~0.5 mJy (Rodighiero et al. 2006), with a peak at ~0.3 mJy, similar to the 15 μm and 12 μm observations. Below 60 μJy, the 24 μm galaxy number counts obtained by the *Spitzer*/MIPS deep surveys (Marleau et al. 2004; Papovich et al. 2004; Chary et al. 2005) face the problem of a confusion limit due to extragalactic sources. Several interpretations propose huge evolution factors in luminosity and/or density. In the *Chandra* Deep Field South survey, the sample of 2600 *Spitzer*/MIPS sources brighter than 80 μJy is interpreted with the comoving IR energy varying as $(1+z)^{3.9\pm0.4}$ (Le Floc'h et al. 2005). The origin of such a high evolution is however not described. More recently, Caputi et al. (2006) analysed the stellar populations of the *Spitzer*/MIPS 24 μm galaxies in the GOODS/CDFS from K_s images. They show evidence for a bump in the redshift distribution at $z = 1.9$, induced by a significant population of galaxies with PAH emission.

The combined *ISO*-ESS survey presented here has a comparable depth (~80% completeness at ~0.7 mJy) and surface area (680 arcmin^2) at 12 μm to the intermediate surveys (Lockman Deep and Marano Deep fields) performed at 15 μm as part of the *ISOCAM* Guaranteed Time Extragalactic Surveys. The specificity of the *ISO*-ESS survey is to provide deep galaxy counts at $\sim 12 \pm 3.5$ μm (*LW10* filter), in a wavelength range where the spectral energy distribution (SED) is dominated by the signatures of PAH emission; it thus strongly constrains the evolution process. The target field is located within the ESO-Sculptor Survey (de Lapparent et al. 2003, 2004), for which deep optical BVR_c magnitudes up to $R_c \leq 23.5$ and spectroscopic redshifts at $R_c \leq 21.5$ have been obtained (Arnouts et al. 1997; Bellanger et al. 1995).

We then model the 12 μm number counts using the new version PÉGASE.3 of the "Projet d'Étude des GAlaxies par Synthèse Évolutive" (Fioc et al. 2007; Fioc & Rocca-Volmerange 1997, 1999b; see also `www2.iap.fr/pegase`), which coherently complements the UV-optical-NIR emission from stars and gas with the mid- and far-infrared emission from dust. The specific goal of our analysis is to predict the mid-infrared number counts using firstly the same scenarios of galaxy evolution by type, with the same number fractions and the same total number densities of galaxies as used for the successful predictions of the UV-optical-NIR deep counts by Fioc & Rocca-Volmerange (1999a). Secondly, if needed, other scenarios are proposed to model the population of ULIRGs able to reproduce the systematic departure observed around 0.3 mJy in mid-infrared surveys.

Section 2 describes the parameters of the *ISO*-ESS field observed with the large pass-band *ISOCAM* LW10/12 μm filter and summarises the data analysis required to extract a catalogue of sources presented in the companion article (Seymour et al. 2007a). The corresponding cumulative and differential galaxy counts at 12 μm are presented in Sect. 3. We resume in Sect. 4 the parameters of two models of evolution scenarios and the observed IRAS luminosity function at 12 μm tentatively used to model galaxy counts. The respective fits of the cumulative and differential counts of the ESO-ESS survey by the two models are compared in Sect. 5. The best model 2 identifies a population of distant ultra bright ellipticals interpreted as distant ULIRGs. Applied to 24 μm number counts from the deep *Spitzer*/MIPS surveys, we show in Sect. 6 that the same population of ultra bright ellipticals also reproduces the 24 μm differential count excess, making our model a robust description. Section 7 presents the cosmic star formation history resulting from the best fit, taking into account the respective contributions per galaxy type. Section 8 discusses the stellar and dust masses of the revealed ULIRG population and the possibility of a hidden AGN. The final section presents our conclusions.

2. Observations and data reduction

The selected field, the ESO-Sculptor Survey (ESS) of faint galaxies, is described in its complete version by de Lapparent et al. (2003). Located near the southern Galactic pole, the observations for the ESS were performed as an ESO key-program, thanks to guaranteed time on the ESO NTT and 3.6 m telescope. Deep CCD Johnson B, V and Cousins R_c magnitudes for nearly 13 000 galaxies to $V \simeq 24$ were obtained over a continuous area of $\sim$0.37 deg^2 (Arnouts et al. 1997). Multi-object spectroscopy has also provided redshifts and flux-calibrated spectra over a sub-area of $\sim$0.25 deg^2 for 617 galaxies with $R_c \leq 20.5$ (92% complete) and 870 galaxies with $R_c \leq 21.5$ (52% complete). The optical star/galaxy separation was performed using the "stellarity" index from the SExtractor software (Bertin & Arnouts 1996). The optical spectra were classified using a principal component analysis (Galaz & de Lapparent 1998). The optical luminosity functions were then measured per galaxy spectral type (de Lapparent et al. 2003) and lead to the detection of a marked evolution in the spiral galaxy populations, characterised by an excess of late spiral and irregular galaxies at $z \simeq 0.5-1.0$ (de Lapparent et al. 2004).

2.1. The ISO survey on the ESS field (ISO-ESS)

The *ISO* observations of the ESS field were performed with the raster mode CAM01 of the *ISOCAM* camera (Cesarsky et al. 1996) on board the *Infrared Space Observatory ISO* (Kessler et al. 2003). The broad-band LW10 filter, with reference wavelength $\lambda_{ref} = 12$ μm and covering the 8.5–15.5 μm interval, was built for a direct comparison with the 12 μm *IRAS* filter (Moneti et al. 1997). The pixel field of view (PFOV) with *ISOCAM* is a 6 arcsec square and the adopted integration time was 5.04 s. per exposure. Ten raster maps were built within the total on-target time of 14 h. All the rasters have $M \times N = 8 \times 8$ pointings each offset by $dM = dN = 60$ arcsec along the axis of the detector. The number of exposures per pointing is $N_{exp} = 13$ and the number of stabilization exposures is $N_{stab} = 10$. The total area of the survey is $\sim$680 arcmin^2 with a maximum exposure time of 1200 s. and an average exposure time of $\sim$660 s per sky pointing.

The *ISO* target field has been selected in the region of the ESO-Sculptor survey where the cirrus emission is minimal (Seymour et al. 2007a). The overlap between the 2 surveys is large, as it represents 90% of the *ISOCAM* survey area and 75% of the ESO-Sculptor spectroscopic area.

2.2. Summary of the data processing

This section is a summary of the data analysis presented in the companion article (Seymour et al. 2007a). The various steps of data processing are (1) deglitching (i.e. cosmic ray subtraction), (2) correction of the long transient behaviour etc. performed by the PRETI software of Stark et al. (1999), and (3) source detection above a noise map, performed using a wavelet analysis technique. The detailed adaptation of the PRETI method to the *ISOCAM* data analysis was published by Aussel et al. (1999). We fine-tuned the astrometry of the 12 μm sources by comparison with matched objects in the 2MASS catalogue, which led to a maximum change of 0.3 arcsec in the position of the 12 μm sources. The subsequent rms offset between the *ISOCAM* 12 μm and the ESS coordinates is 2 arcsec, with no systematic offset. The star/galaxy separation was performed by a detailed analysis of the near-infrared (NIR) and optical colour–colour diagrams. We then derived an empirical flux calibration from a subset of stars in our sample. This calibration was based on fitting the optical-NIR counterparts of the stellar data with stellar spectrum templates compiled in the PÉGASE library and then using the optical/infrared relations from IRAS data to predict the true infrared fluxes of stars in our field. This procedure took advantage of the deep photometric ESS survey in the optical. Our flux calibration is robust as it was carried out using two different colour–colour relations and empirical calibration using well-known stellar templates. The final catalogue of 142 sources with *ISO* fluxes is listed in the companion article and contains 22 stars and 120 galaxies. As expected, only a small fraction of the MIR sources are stars.

2.3. Large-scale distribution of the ISO-ESS sources

With an average exposure time of 11 min by pointing, our *ISO*-ESS survey is as deep as the Lockman Hole Deep survey from the *ISOCAM* Guaranteed Time Extragalactic Survey (Elbaz et al. 1999), but it is over a 33% larger area of $\simeq$680 arcmin^2. Despite its significant area, the *ISO*-ESS map reveals the inhomogeneity of the projected distribution of MIR sources. The large-scale distribution of galaxies in the ESS shows the alternation of sharp walls and voids (Bellanger & de Lapparent 1995). For $H_0 = 65$ km s^{-1} Mpc^{-1}, de Lapparent & Slezak (2007) measure a comoving correlation length of $\sim$5.5 Mpc at the median redshift $z \sim 0.3$ of the *ISO*-ESS galaxies; the right ascension transverse extent of the survey ($\sim$11 Mpc) thus corresponds to approximately twice the galaxy correlation length. Because the MIR sources are likely to follow the clustering of optical galaxies, large-scale fluctuations are naturally expected. These are smoothed out, however, when calculating the *ISO*-ESS galaxy counts summed over the whole redshift range of the survey.

3. Faint galaxy counts at 12 μm

The *ISO*-ESS sample consists of sources with a detection level equivalent to 5σ and is complete to 1.29 mJy. At fainter flux densities, the correction for incompleteness in the interval 0.31−1.29 mJy is computed by two independent methods based on stars and galaxies in the optical. Both approaches take advantage of the deep ESS optical survey, which contains counterparts to all sources detected by *ISOCAM* down to 0.31 mJy (in the common area to both surveys), and they yield incompleteness corrections that are in good agreement (see Fig. 7 in companion paper). Here, we correct the galaxy number counts using the incompleteness correction derived from the stars, as it is least affected by the large-scale clustering in the ESS sample (see Sect. 2.3). Figure 1 shows the distribution by type of the 77 *ISO*-ESS galaxies that have measured redshifts from the optical survey (de Lapparent et al. 2003). It shows that spirals Sb and Sbc are the most numerous galaxies detected in the MIR. It also confirms that gas-poor normal ellipticals are essentially undetected. The ESS spectral classification used the code PÉGASE.2 (Fioc & Rocca-Volmerange 1997). However, the sample in Fig. 1 is incomplete, with only 77 galaxies having a measured redshift. Among the 104 ESS galaxies detected at 12 μm, the 27 objects with no redshift measurement could be at higher redshift or belong to a new type. We therefore adopt the "optical" density fractions derived from the faint count analysis in the UV-optical-near IR ($\simeq$27%, 30%, and 43% for early-, intermediate-, and late-type galaxies, respectively) by Fioc et al. (1999a), in agreement with de Lapparent et al. (2003) in the Sculptor field.

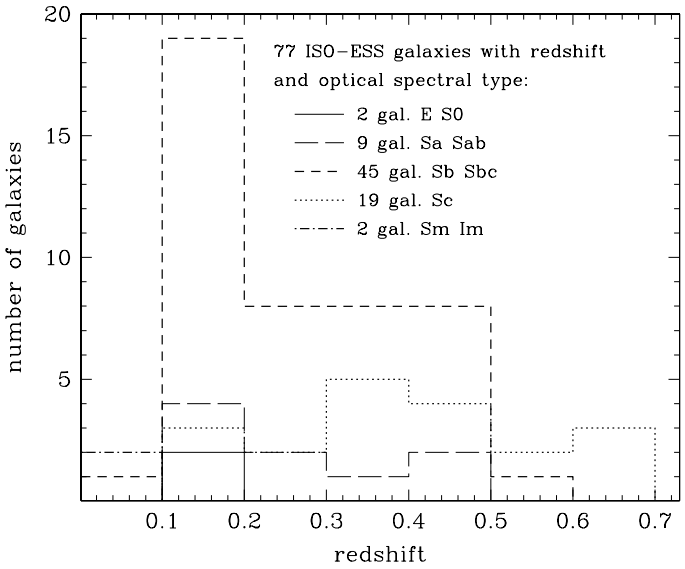

Fig. 1. The distribution by types of the ($R < 20.5$) *ISO*-ESS galaxies, derived from the optical spectral classification (de Lapparent et al. 2003). The dominant population is Sb-Sbc spirals, confirming that ellipticals are rarely detected at 12 μm. Note, however, that among the 104 galaxies detected at 12 μm in the area common to both surveys, only 77 have ESS spectroscopic information (hence redshift and spectral type), leaving room for the discovery of new populations and signatures of evolution.

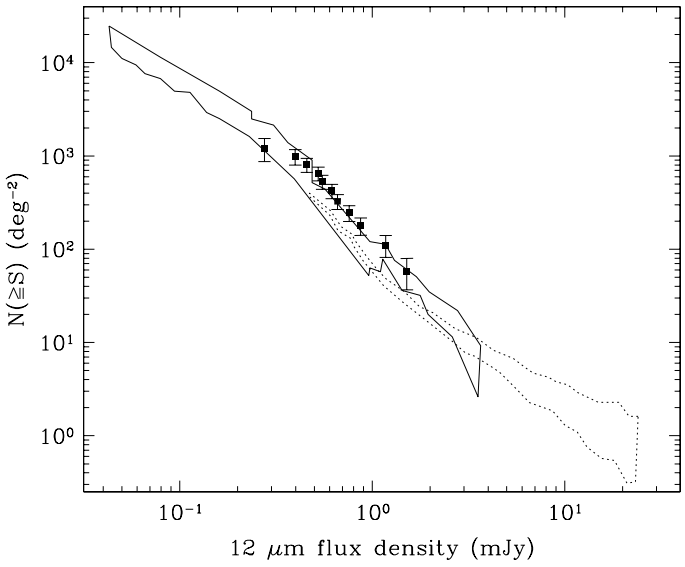

Fig. 2. Cumulative 12 μm galaxy counts observed with the *LW10* filter from the *ISO*-ESS survey, plotted as full squares with error bars. The other *ISOCAM* 15 μm surveys are also plotted: the compilation by Elbaz et al. (1999) as a solid line contour, which covers the Lockman Hole (Rodighiero et al. 2004), the Marano field (Aussel et al. 1999), and the HDF North and South fields (Altieri et al. 1999) to various depths; the number-counts from the ELAIS survey (La Franca et al. 2004) are shown as a dotted line. The 15 μm flux densities are corrected to 12 μm, see text for details.

3.1. Cumulative galaxy number counts $N(\geq S_\nu)$ at 12 μm

We then derive the number of detected *ISO*-ESS galaxies as a function of 12 μm flux density. The detections are binned in 11 flux-density intervals, chosen so that each bin contains 10−12 more sources than the previous one. The resulting cumulative source counts $N(\geq S_\nu)$ (commonly referred to "integrated counts" in the literature), where S_ν is the 12 μm flux in mJy, derived after correction for incompleteness, are shown in Fig. 2. Corrections are estimated by assuming Poisson fluctuations in the number of detected galaxies and by taking the uncertainty in the incompleteness correction into account; the horizontal error bars are not plotted as they are smaller than the size of the symbols. The large error bars in the high flux point at $S_\nu \simeq 1.4$ mJy result from the small number of galaxies (10) detected at these high flux densities: this is evidently due to the limited area of the *ISO*-ESS field.

We overlay in Fig. 2 the results from the compilation of *ISOCAM* 15 μm surveys obtained in the *LW3* filter as published by Elbaz et al. (1999): they cover the Lockman Hole, Marano and HDF North and South fields (Rodighiero et al. 2004; Aussel et al. 1999; Altieri et al. 1999) at various depths. We also plot for comparison the results from the ELAIS survey, also observed at 15 μm (La Franca et al. 2004). When plotting the 15 μm number counts, the flux density is converted into the LW10 12 μm band using the respective central wavelengths of the two filters and assuming a flat spectrum in flux (that is, a constant product of the frequency by the flux density); the correction is small, a factor 12/15 = 0.8. We do not correct the galaxy flux densities from 15 μm to 12 μm because the filters are wide and very close to each other in wavelength (they actually overlap slightly).

Figure 2 shows that our data are in good agreement with the surveys compiled by Elbaz et al. (1999), including the deepest samples. In particular, the faint-end slope of the *ISO*-ESS cumulative counts is similar to that of the ultra-deep survey obtained on the cluster-lens A2390 by Altieri et al. (1999) in their common flux density interval, despite the narrow pencil-beam geometry of the latter survey. The *ISO*-ESS counts are also consistent with the brighter galaxy survey from La Franca et al. (2004).

3.2. The Euclidean-normalized differential counts

The differential galaxy counts $-S^{2.5}\mathrm{d}N/\mathrm{d}S$ of the *ISO*-ESS survey at 12 μm, normalised to those for an Euclidean Universe are presented in Fig. 3. A wider binning than in Fig. 2 is adopted, with 23−25 galaxies per bin. The error bars take into account Poisson error in the number of actually detected sources, combined with the uncertainties in the incompleteness correction and in the flux density of each detected source; as for the cumulative counts, the flux error bars are not plotted as they are smaller than the size of the symbols. The Euclidean normalisation is adopted so that for a static universe with a non-evolving population of objects and a constant luminosity function, the Euclidean normalised galaxy counts would follow a horizontal line.

The differential number counts from the surveys at 15 μm (with flux density converted into the 12 μm band, see previous section) are also plotted in Fig. 3 (ELAIS-S1, Pozzi et al. 2003; A2390, Altieri et al. 1999; HDF North, Aussel et al. 1999; HDF South, Marano FIRBACK Ultra Deep field, Marano Ultra Deep ROSAT field, Marano Deep field, Elbaz et al. 1999; Lockman Deep and Lockman Shallow field, Rodighiero et al. 2004). As for cumulative counts, the 15 μm counts are corrected to 12 μm (see Sect. 3.1). Note that our faintest bin (at ∼0.3 mJy) is very uncertain due to incompleteness, which may explain the downward shift for this last point. For clarity we do not include the 12 μm galaxy counts from Clements et al. (1999), which show a large scatter, probably due to poor statistics (3−5 objects per bin). They may also suffer from contamination by a few stars at

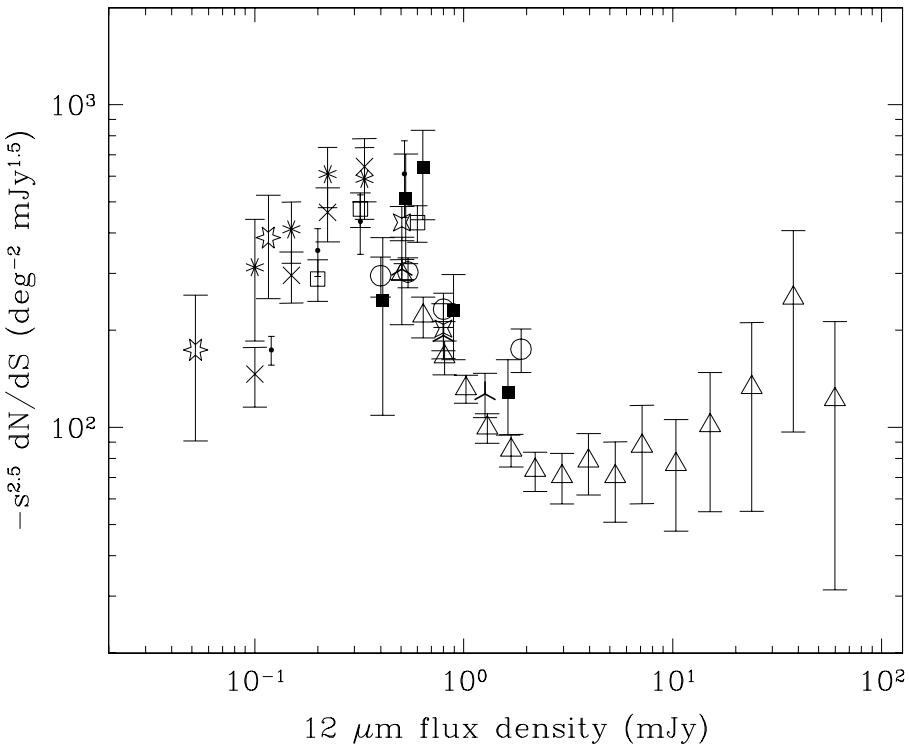

Fig. 3. The *ISO*-ESS 12 μm differential counts normalised to the Euclidean case, plotted as filled squares (note that $-S^{2.5}\mathrm{d}N/\mathrm{d}S$ is positive). The other 15 μm surveys are also shown: ELAIS-S1 (Pozzi et al. 2003, triangles); through the cluster-lens A2390 (Altieri et al. 1999, 6-pointed open star), HDF North (Aussel et al. 1999, crosses); HDF South (asterisks), Marano FIRBACK Ultra Deep field (open squares), Marano Ultra Deep ROSAT field (points), Marano Deep field (open circles), all published in Elbaz et al. (1999); Lockman Deep field (4-pointed open star), Lockman Shallow field (3-pointed heavy cross), both from Rodighiero et al. (2004). See text for the details of the correction from 15 μm to 12 μm.

the bright end: the authors admit that there is at least one star in their galaxy counts (Clements et al. 2001).

In Fig. 3, the *ISO*-ESS counts show a strong departure from Euclidean no-evolution models at faint fluxes (<1 mJy), with a very steep super-Euclidean slope. The same behaviour is observed in all the other surveys plotted in the figure, showing agreement among the 15 μm surveys and with our 12 μm survey. The low value of our last point at faint fluxes (~0.3 mJy) is due to the large uncertainty in the incompleteness correction. In the following, we address the issue of the origin of the excess counts by modeling the faint galaxy counts with the evolutionary code PÉGASE.

4. Modeling MIR galaxy counts per type with the code PÉGASE.3

In the following we adopt a flat Universe with the standard cosmological parameters: $H_0 = 72$ km s^{-1} Mpc^{-1}, $\Omega_\mathrm{M} = 0.3$, $\Omega_\Lambda = 0.7$ (Spergel et al. 2003).

4.1. The code PÉGASE.3

The new evolutionary code PÉGASE.3 (Fioc et al. 2007) is an extension to the dust emission wavelength range of the code PÉGASE.2 (Fioc & Rocca-Volmerange 1997, 1999b, see also `http://www2.iap.fr/pegase`). The SEDs of reddened galaxies are consistently computed from the far-UV/optical/near-IR to mid-IR and FIR (far-infrared) domains. PÉGASE.3 calculates, in a coherent manner, the stellar emission, extinction, metal-enrichment, dust mass, and the emission of grains statistically heated by the radiation field. Two distinct dust media (interstellar medium and HII regions) are considered. As in PÉGASE.2, radiation transfer is computed in the two geometries (slab and spheroid) appropriate for disk galaxies and ellipticals. Temperature fluctuations of the polycyclic aromatic hydrocarbons (PAH), as well as graphite and silicate grain properties, are

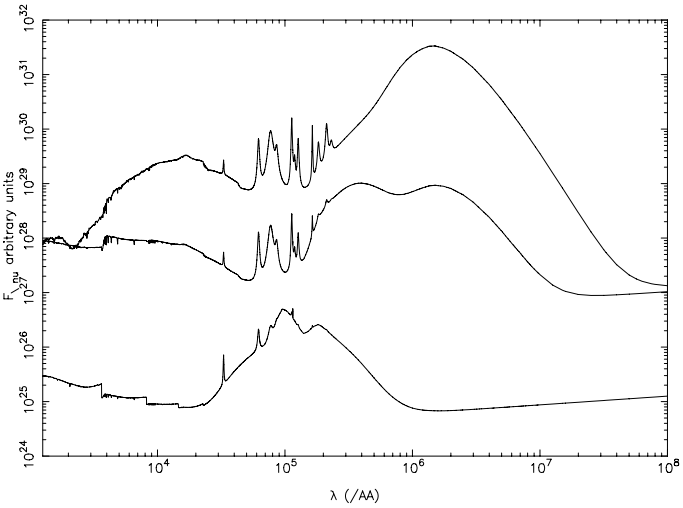

Fig. 4. Example of the strong evolution in the SEDs predicted by PÉGASE.3 for a star forming galaxy spiral Sc at various ages (increasing upwards), in the wavelength interval 1000 Å to 1 cm. (See more details in Fioc et al. 2007.)

derived with the method of Guhathakurta & Draine (1989). For illustration, Fig. 4 shows the strong evolution of the spectral energy distribution (SED) of the spiral Sc template (especially in the MIR between 10 μm and 20 μm) at various ages.

4.2. Evolutionary scenarios of galaxies and relative number density fractions

4.2.1. Model 1: "normal" evolved types

In a first step, we adopt the same set of evolutionary scenarios of "normal" galaxies previously determined with the code PÉGASE.2 (Fioc & Rocca-Volmerange 1997) which fit the colours of nearby galaxies by type and the deepest

Table 1. Characteristic luminosity L_* in units of $L_\odot$ at 12 μm (Col. 3) and 24 μm (Col. 4) of the $z = 0$ luminosity functions used here, as a function of galaxy type (Col. 1). Column 2 gives the value of the parameter p_2, the rate defined by $SFR_i(t) = M_{\rm gas}(t)/p_2$. Galactic winds occur at an age of 3 Gyr in ellipticals of type E and ULIRG, and at 1 Gyr in ellipticals of type E2; there are no galactic winds in spirals. Infall time scale of ULIRGs is 100 Myr as for ellipticals of type E or E2; it regularly increases for spirals from 2.8 Gyr (Sa) to 8.0 Gyr (Im) (see text for details and references). The $L_*(12\ \mu{\rm m})$ for the normal types (other than ULIRG) are derived from the $L_*(B_J)$ of the observed optical luminosity functions from Heyl et al. (1997) and the $B_J - 12\ \mu$m and $B_J - 24\ \mu$m colours, in the AB magnitude system, are computed at $z \simeq 0$ with PÉGASE.3 (Cols. 5 and 6). The value of $L_*(12\ \mu{\rm m})$ assigned to Sbc galaxies, the brightest emitters in this band, is that of the observed luminosity function measured with *IRAS* (Rush et al. 1993; Shupe et al. 1998); the same offset as for Sbc is then applied to all types. The last two columns show the adopted number density fraction by type: model 1 (normal galaxies only, Col. 7) uses the type distribution derived from the UV-optical-near IR faint counts (Fioc et al. 1999a) while model 2 (normal galaxies + ULIRGs, Col. 8) is built by replacing 1/3 of normal dust-poor ellipticals (9% of all galaxies) with ultra luminous elliptical galaxies (called ULIRGs). These last galaxies evolve as dusty ellipticals, they are ≃2.5 to ≃5 mag brighter than normal ellipticals (depending on wavelength), and are thus as luminous as spirals Sbc in the mid-IR at $z = 0$. The number densities for the other galaxy types are identical in both models.

Type	p_2 (Myr)	$\log_{10}$ $[L_*(12\ \mu{\rm m})/L_\odot]$	$\log_{10}$ $[L_*(24\ \mu{\rm m})/L_\odot]$	Colour $B_J - 12\ \mu$m $_{AB}$	Colour $B_J - 24\ \mu$m $_{AB}$	Model 1 normal only	Model 2 normal + ULIRGs
ULIRG	100	9.9	9.7	–	–	0%	9.0%
E	100	8.9	7.7	–1.00	–2.60	9%	0%
E2	300	9.0	7.8	–1.20	–2.82	17.5%	17.5%
Sa	1400	9.0	8.8	–0.45	+0.21	7.9%	7.9%
Sb	2500	9.4	9.2	+0.37	+1.28	7.9%	7.9%
Sbc	5714	9.8	9.6	+1.38	+2.30	7.9%	7.9%
Sc	10000	9.6	9.4	+1.57	+2.46	16.6%	16.6%
Sd	14286	9.6	9.4	+1.61	+2.48	16.6%	16.6%
Im	16000	8.8	8.5	+1.57	+2.42	16.6%	16.6%

multi-wavelength (B_J, U (and $F300W$), I, and K) faint galaxy counts in the UV-optical-NIR ranges (Fioc & Rocca-Volmerange 1999a). This set corresponds to the 8 following types: irregular magellanic Im; spirals Sd, Sc, Sbc, Sb, Sa; and ellipticals E2 and E). We use the same parameter set with the new version PÉGASE.3 (Fig. 4) and compute the continous SEDs of each type, extended to the mid- and far-IR, taking stellar and dust emissions into account as well as coherent absorption. The initial mass function is from Rana & Basu (1992) for each type. These templates are also able to predict photometric redshifts up to $z = 4$ with an accuracy $\sigma_z \simeq 0.1$ (Le Borgne & Rocca-Volmerange 2002). Therefore the evolution scenarios are considered as robust. The main parameters (star formation law, initial mass function, galactic winds and astration rate) are listed for each type in Fioc & Rocca-Volmerange (1997) and Le Borgne & Rocca-Volmerange (2002). Star formation rates are proportional to the current gas mass density, a highly conservative assumption. The astration parameter p_2^{-1} varies with galaxy type. The current gas content $M_{\rm gas}(t)$ is ruled by star formation, stellar ejecta, galactic winds, and infall rates as described in Fioc & Rocca-Volmerange (1997); the adopted values by type are recalled in Table 1.

In Table 1, we present the $z = 0$ characteristic luminosities $\log(L_*(12\ \mu{\rm m})/L_\odot)$ and $\log(L_*(24\ \mu{\rm m})/L_\odot)$ adopted for the various galaxy types. We compute $L_*(12\ \mu{\rm m})$ and $L_*(24\ \mu{\rm m})$ from the $L_*(B_J)$ values of the optical luminosity functions by types (Heyl et al. 1997), used to fit the faint optical counts (see Table 1 of Fioc & Rocca-Volmerange 1999a), and the colours $B_J - 12\ \mu$m and $B_J - 24\ \mu$m from PÉGASE.3 at $z = 0$ for each galaxy type (Fioc et al. 2007). The filter 12 μm means *ISO*/LW10 and 24 μm means *Spitzer*/MIPS 24 μm; B_J is the blue Kodack IIIa-J plus GG395 corrected filter (Couch & Newell 1980). The filter corrections from *IRAS*/12 μm to *ISO*/LW10 and from *IRAS*/25 μm to *Spitzer*/24 μm are taken into account by the code. Among normal galaxies at $z \simeq 0$, spirals Sbc are the brightest emitters at 12 μm and 24 μm and also the most numerous (see Fig. 1). We therefore assign to type Sbc the characteristic luminosities $\log(L_*(12\ \mu{\rm m})/L_\odot) = 9.8$ and $\log(L_*(24\ \mu{\rm m})/L_\odot) = 9.6$ derived from the observed $z \simeq 0$ luminosity functions measured by Rush et al. (1993) and by Shupe et al. (1998), respectively. We then scale the MIR luminosities of all the other types accordingly.

Because the evolutionary scenario of ellipticals (see Fig. 3a of Rocca-Volmerange et al. 2004) may play a specific role in the interpretation of observations of the ultra-luminous infrared galaxies (ULIRGs), defined as galaxies with infra red luminosities $\geq 10^{12}\ L_\odot$, it deserves more attention. The intense star formation rate (low p_2 value) in the first Gyrs is fueled by a high infall rate from the gas reservoir. The activity is so intense that a huge dust mass is formed at early epochs from stellar ejecta, specifically from massive supernovae SNII. In normal elliptical galaxies, the star formation activity is supposed to be halted when strong galactic winds produced by the bulk of supernovae expell all the gas and dust content from the galaxy. Most of stars and dust are already formed when the galaxy age is about 1 Gyr, corresponding to $z \simeq 4$ in the adopted cosmology. "Normal" ellipticals contribute very little thereafter to the infrared emission, as they are largely dust-free from this age to the present time ($0 \leq z \leq 4$). This scenario at $z = 0$ matches the observation that the cold grain component (~50 K) in elliptical galaxies has almost no contribution to the MIR flux (Xilouris et al. 2004).

Column 7 of Table 1 gives the relative number fractions of galaxy types for model 1, as derived from the UV-optical-near IR. This model has no "ULIRG"component and is thus composed only of normal types (26.5% ellipticals (E + E2), 23.7% Sa to Sbc spirals, 33.2% Sc, Sd spirals and 16.6% irregulars), which were found to fit the deepest UV-optical-near IR faint galaxy counts (see Fig. 5 from Fioc & Rocca-Volmerange 1999a).

4.2.2. Model 2: over-luminous dusty ellipticals as ULIRGs

Column 8 of Table 1 describes our model 2 with "ULIRG" which we use to adjust the MIR galaxy counts. In this model, 1/3 of the ellipticals have over-luminous MIR luminosities given

by $\log(L_*(12\ \mu\mathrm{m})/L_\odot) = 9.9$ and $\log(L_*(24\ \mu\mathrm{m})/L_\odot) = 9.7$, which correspond to the observed characteristic $L*$ of the MIR luminosity functions at these two wavelengths. At $z = 0$ and in the MIR, they are as bright as Sbc spirals, and brighter by 2.5 mag at 12 μm and 5 mag at 24 μm than normal ellipticals, whatever their type (E2, E). However, they follow the evolution scenario of elliptical galaxies of type E, with the same astration rate p_2^{-1}, infall and galactic winds at the same age.

These overluminous ellipticals, forming large masses of dust and stars at early epochs, become much brighter at high z than spirals. Due to their positive k-corrections at high redshift, their intense stellar emission appears in the mid-IR. As a consequence, our model does not need any additional starburst as in the typical case of M 82 (Silva et al. 1998). Our model remains compatible with occasional starbursts of short duration ($<10^8$ yrs), concerning a low mass fraction relative to the massive underlying elliptical galaxy.

Column 8 of Table 1 lists the number fractions for model 2. The population of ULIRG/dusty massive ellipticals corresponds to 9% of the total number of galaxies. The number of normal dust-poor ellipticals is then reduced to only 17.5% (only 2/3 of the ellipticals observed in the visible). The rest of the galaxies are normal; model 2 therefore respects the majority of fractions by type derived from the UV-optical-near IR galaxy counts.

4.2.3. The *k(z)* and *e(z)* corrections per type

To calculate the apparent magnitudes at high z, the evolutionary $e(z)$ and cosmological $k(z)$ corrections are computed for each type, as in Rocca-Volmerange & Guiderdoni (1988), and are applied to the $z = 0$ SEDs:

$$m(z, t_z) = M(0, t_0) + k(z) + e(z) + 5\log_{10}[D_\mathrm{A}(1+z)^2] + 25 \quad (1)$$

where D_A is the angular diameter distance in Mpc, $D_\mathrm{A}(1+z)^2$ the luminosity distance, t_z and t_0 the cosmic times at z and $z = 0$; internal extinction is taken into account in our scenarios; no Galactic extinction term is added, because our deep survey is performed in a region of weak galactic absorption.

The same formation redshift of $z_\mathrm{for} = 10$ is arbitrarily adopted for all galaxy types, following the most distant galaxies discovered at $z > 6$ (Hu et al. 2002; Chary et al. 2005).

4.3. The 12 μm luminosity function by type at z = 0

We take advantage of the quasi-similarity of the two filters *IRAS*/12 μm and *ISOCAM*/LW10/12 μm (the flux differences are <10%, see companion article) and use the local 12 μm luminosity function measured by Rush et al. (1993) from the *IRAS* catalogue (this measurement was later confirmed and extended to fainter fluxes by Fang et al. 1998),

$$\phi_0(L) = C\left(\frac{L}{L_*}\right)^{1-\alpha}\left(1+\frac{L}{\beta L_*}\right)^{-\beta}. \quad (2)$$

We adopt the values $\alpha = 1.7, \beta = 3.6$ measured by Rush et al. (1993) for the non-Seyfert galaxies, which include *all* galaxy types detected at $z = 0$. As shown in Table 1, the $L_*(12\ \mu\mathrm{m})$ adopted for each galaxy type are derived by combining the optical $L_*(B_J)$ (Heyl et al. 1997) with the $B_J - 12\ \mu$m colors predicted by the code PÉGASE.3 (Cols. 5 and 6). We assign to Sbc galaxies, the brightest emitters in these bands, the *IRAS* values of $L_*(12\ \mu\mathrm{m})$ from the observed luminosity functions (Rush et al. 1993; Fang et al. 1998). The same offset as for Sbc is then applied to all types.

5. Results of galaxy count model at 12 μm

5.1. Cumulative and differential counts from PÉGASE.3 at 12 μm

Faint galaxy counts are computed following the already published formalism (see Sect. 2 in Guiderdoni & Rocca-Volmerange 1990) which assumes that the number of galaxies of each type is conserved. Comparison of the *ISO*-ESS number counts with the predictions of PÉGASE.3 at 12 μm is shown in Fig. 5 for cumulative counts, and in Fig. 6 for Euclidean-normalised differential counts (solid line in both graphs); the number counts from the 12 μm *ISO*-ESS, and from the published 15 μm surveys are also shown with the same line/symbol coding as in Figs. 2 and 3. Figure 5 shows that the model with ULIRGs agrees well with the *ISO*-ESS cumulative counts. After colour correction, it also fits the deep *ISO* counts at 15 μm as well as the ultra-deep survey down to 0.05 mJy in the cluster-lens A2390 (Altieri et al. 1999; Lemonon et al. 1998), implying that there is no significant number density variation between the field and clusters. The differential counts (Fig. 6), which are more constraining, remain in reasonably good agreement with the data, in particular at faint fluxes. The Euclidean-normalized differential counts predicted with PÉGASE.3 do show the departure from the Euclidean cosmology (horizontal line) observed at 0.3 mJy in all the data samples. This bump is not due to the evolution of bright spirals, nor to normal early-type galaxies, but only to the evolution of the third of elliptical galaxies (9% of all galaxies) which are dusty ultra-bright ellipticals. From a few 0.1 to $\simeq$1 mJy, only the slope of the Marano Deep Field is respected by models, in excess relative to other observations by a factor 2. The model prediction with only the universe expansion effect (obtained by applying only the $k(z)$ corrections to the SEDs) is also plotted in Figs. 5 and 6 as a dashed line: it is noticeably insufficient to reproduce the marked excess counts and the peak at 0.3 mJy. We also checked that the model without any correction (i.e. no $k(z) + e(z)$ corrections applied to the SEDs), which only includes the evolution of the comoving elemental volume, yields decreasing differential counts which are incompatible with observations; this curve is shown in Figs. 5 and 6 as a dotted line.

Note that the comparison of the observed *ISO*-ESS counts with the Euclidean case is more meaningful in the flux range where the number density is the highest. When galaxy numbers are statistically too small, error bars are large as shown at fluxes higher than 10 mJy and $\leq$0.1 mJy. Finally we can ask whether the normal spirals which are ultra-luminous in the MIR ($\log(L_*(12\ \mu\mathrm{m})/L_\odot) = 9.8$ and $\log(L_*(24\ \mu\mathrm{m})/L_\odot) = 9.6$ (see Table 1) can also reproduce the bump of MIR counts as well as models with ULIRGs. At 12 μm, the normal populations, dominated in the MIR by spirals Sbc are quite unable to reproduce the excess counts of the MIR surveys (Figs. 5 and 6, left), even by adding 9% to the ~57% of normal spirals in place of gas-poor elliptical galaxies.

6. Galaxy count model at 24 μm

The deepest *Spitzer*/MIPS 24 μm surveys are in the area of the Chandra Deep Field South (Papovich et al. 2004). The corresponding galaxy counts (cumulative, shown in Fig. 7, and differential normalized to the Euclidean case, shown in Fig. 8) are characterised by a typical bump of the galaxy density between 3 and 0.03 mJy, similar to what is observed in the 12 μm and

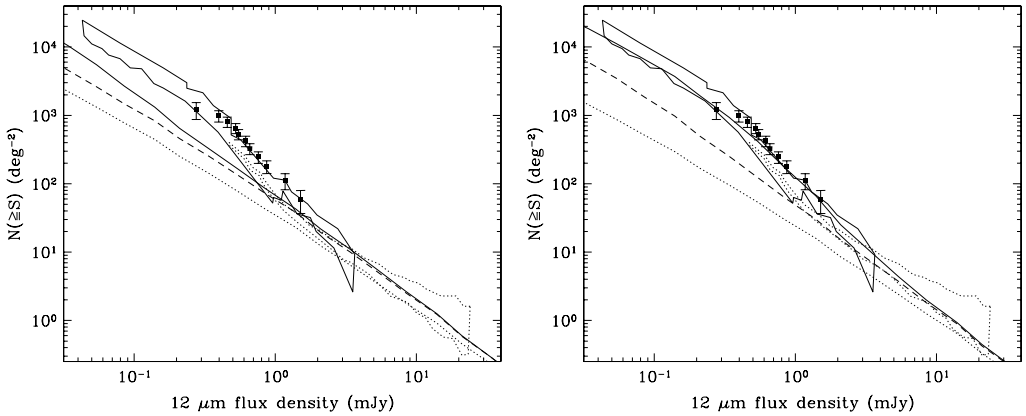

Fig. 5. The predictions of 12 μm cumulative galaxy counts (heavy line) calculated from model 1 of normal galaxies (*left*) and model 2 with 9% of ULIRGs (*right*): see Table 1, Cols. 7 and 8. They are compared to the observed 12 μm cumulative counts from the *ISO*-ESS survey (black squares). The models with the cosmological k-correction only (no evolution correction: heavy dashed line) and the models with only the elemental comoving volume effect (dotted line) are also plotted for comparison. The faint counts from the 15 μm surveys are shown with the same line coding as in Fig. 2.

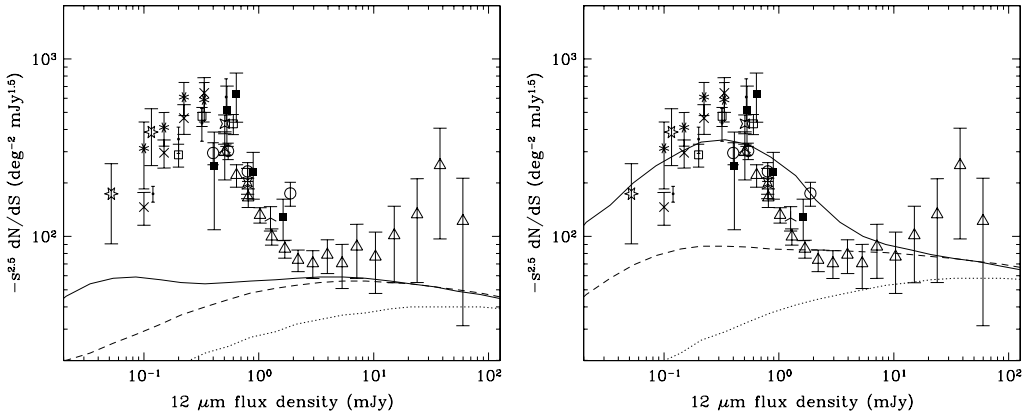

Fig. 6. The predictions of Euclidean-normalised differential 12 μm galaxy counts, calculated with model 1 (normal, *left*) and model 2 (including ULIRGs, *right*) using PÉGASE.3 (solid line), are compared to the observed differential counts at 12 μm from the *ISO*-ESS survey (black squares). The cases without evolution (only cosmological k-correction) are shown with a dashed line, the case without $k + e$ corrections (only the comoving volume effect) with a dotted line. The symbol coding for the 15 μm surveys is the same as in Fig. 3.

15 μm counts. This evolution signature of the 24 μm counts is confirmed by Marleau et al. (2004) and Chary et al. (2004). More recently, in the GOODS-ELAIS-N1 field, Rodighiero et al. (2006) have lowered the confusion limit by about 30−50% using a deblending technique, which leads to a decrease in the bright differential counts by a factor ∼3, and an increase in the count slope at faint fluxes. The statistics of the 24 μm observations are poor for flux densities >10 mJy and the samples suffer from incompleteness for fluxes <80 μJy.

6.1. The local IRAS/25 μm luminosity function

To model the *Spitzer*/24 μm counts, we use the *IRAS*/25 μm luminosity function (corrected for 24 μm) as measured by Shupe et al. (1998),

$$\phi_0(L) = C\left(\frac{\alpha}{x} + \frac{\beta}{1+x}\right) x^{1-\alpha}\,(1+x)^{-\beta}, \qquad (3)$$

where $x = L/L_*$, and the parameters are $\alpha = 0.437$ and $\beta = 1.749$ for all galaxy types. As for 12 μm, we computed $L_*(24\ \mu\mathrm{m})$ by types from the Heyl et al. (1997) $L_*(B_J)$ and the $B_J - 24\ \mu$m colour computed with PÉGASE.3 (including filter correction from *IRAS*/25 μm to *Spitzer*/24 μm). We assigned the value of $L_*(24\ \mu\mathrm{m})$ derived from Shupe et al. (1998) to spirals Sbc. The same offset as for Sbc was applied to all types. The resulting values of the characteristic L_* and the corresponding fractions per galaxy type are listed in Table 1.

6.2. Cumulative and differential counts with PÉGASE.3 at 24 μm

We modeled the faint galaxy counts through the *Spitzer*/24 μm filter with the code PÉGASE.3 and the same evolving galaxy population (evolutionary scenarios, density fractions) as already used to predict the 12 μm counts. Figures 7 and 8 compare models 1 and 2 with the cumulative and differential number counts, respectively, obtained by Papovich et al. (2004). As for the 12 μm counts, the 24 μm cumulative counts are well-reproduced from the faintest flux up to a few mJy. Figure 8 shows that the marked steepening of the differential counts, normalised to Euclidean, and the subsequent decrease at faint fluxes are predicted by PÉGASE.3, with a peak at ∼0.3 mJy as observed. Note that the departure of the model from the observations at bright and faint fluxes agrees well with the data corrected for incompleteness and deblending (see Rodighiero et al. 2006). Once again, the fit is more meaningful in the flux range where the number density is the highest, as objects observed at high fluxes in the survey area are rare. Moreover, for the 24 μm filter, the k-correction is negative at $z < 2$ as shown in Fig. 4

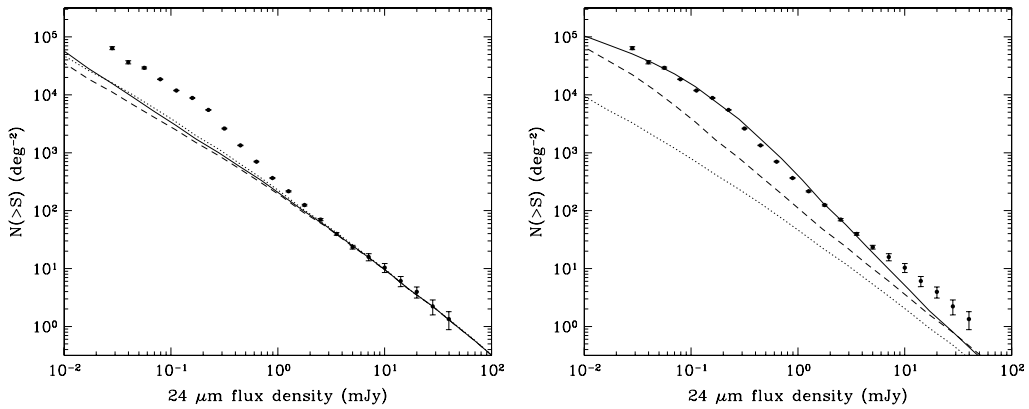

Fig. 7. Cumulative 24 μm faint galaxy counts (solid line) predicted by model 1 (normal, *left*) and model 2 (with ULIRGs, *right*) using PÉGASE.3 (the same models as for the interpretation of the *ISO* 12 μm counts), are compared to the *Spitzer*/MIPS/24 μm observations by Papovich et al. (2004). The luminosity function is from *IRAS*/25 μm (Shupe et al. 1998). As in previous figures, the dashed line is for counts taking into account only the *k*-correction and volume expansion effect, while the dotted line corresponds to the comoving volume correction only (no $k+e$ correction).

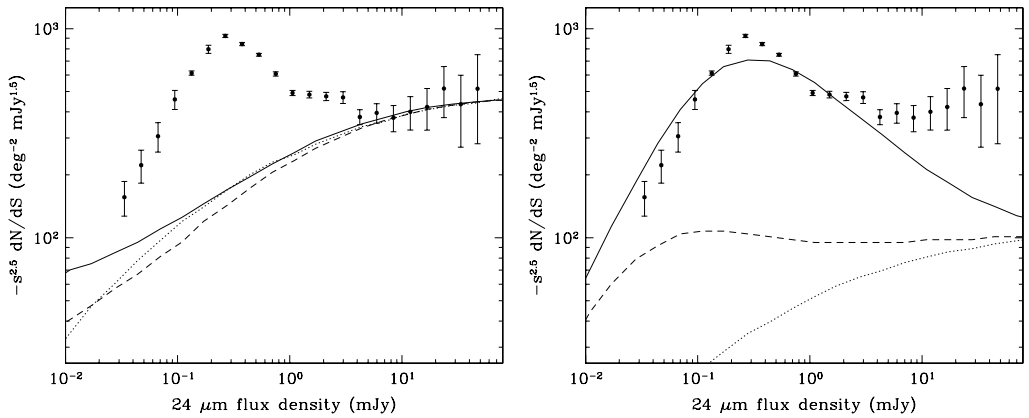

Fig. 8. The differential 24 μm faint galaxy counts computed with PÉGASE.3 (solid line) for model 1 with only normal galaxies (*left*) and model 2 with ULIRGs (*right*), both compared to the *SPITZER*/MIPS/24 μm observations of Papovich et al. (2004). The other symbols are identical to the previous figure. For the 24 μm filter, the *k*-correction line (dashed line, *left*) appears below the comoving volume line because the *k*-correction is negative, as shown by the SEDs displayed in Fig. 4.

by the SED slope from 24 μm to $\simeq$8 μm. In contrast to the study by Gruppioni et al. (2005), based on the flux density ratio $S_{24\ \mu m}/S_{15\ \mu m}$, our model does not require a population of additional starbursts, but rather the very strong evolution factor at high redshift of the star formation rate of elliptical galaxies as presented below.

7. The cosmic star formation rate SFR(z) per type

The models of galaxy populations that simultaneously fit the 12 μm and 24 μm galaxy counts can be used to predict the cosmic star formation rate at high z. We then compute the global star formation rate $SFR(z)$ as

$$SFR(z) = \Sigma_i\ SFR_i(z), \quad (4)$$

where $SFR_i(z)$ is the star formation rate per galaxy type i. The total cosmic $SFR(z)$ and SFR by groups of galaxy type are presented in Fig. 9 in arbitray units (mass per year per volume unit). We distinguish group 1 of E/SO galaxies that shows a striking high SFR between $z > 4$ and the redshift of formation ($z_{\rm for} = 10$): the major bulk of stars has been formed at early epochs before the galactic wind episode. Then group 2 of early spirals (Sa-Sbc), which is dominant from $z = 0.6$ to $z \sim 4$ with a predicted SFR that increases from $z = 0$ to 1 by a factor of $\sim$10, as found by Lilly et al. (1996), Madau et al. (1996), Connolly et al. (1997), mainly from the I-band selected CFRS observations. Finally group 3 of late-type spirals and irregulars (Sc-Im) is dominant from $z \sim 0$ to $z \simeq 0.5$ but has the faintest SFR at $z > 2$.

Because ULIRGs follow the SFR scenario of ellipticals, both normal ellipticals and ULIRGs are represented by the same line (E/S0) in Fig. 9. This hypothesis, fully justified if the origin of the huge luminosity of ULIRGs is not stellar (i.e. if it is due to an active nucleus), emphasises that the star formation history shown in Fig. 9 is a lower limit because it does not include any possible contribution from starbursts caused by interactions. Our model could however accept some such occasional starbursts as seen in nearby ULIRGs, as long as they only represent a few percent of the total stellar mass and are sufficiently short to not be representative of a population.

The evolution of the SFR is different in the two groups Sa-Sbc and Sc-Im. Between $z \simeq 1.5$ and $z = 0$, which corresponds to ages of $\simeq$6 to 13 Gyr, the star formation rate of a 10^{11} $M_\odot$ Sa spiral decreases from $\simeq$20 to 2 $M_\odot$ yr^{-1} at $z = 0$. In the same redshift interval, the star formation rate of a less-evolved Sc spiral with the same mass increases from $\simeq$3 to 4.5 $M_\odot$ yr^{-1}. This is consistent with the local observations: at $z = 0$, the current mean SFR of galaxies is $\simeq$5 $M_\odot$ yr^{-1} for late spirals of 10^{11} $M_\odot$ (and $\simeq$0.5 $M_\odot$ yr^{-1} for 10^{10} $M_\odot$ irregulars);

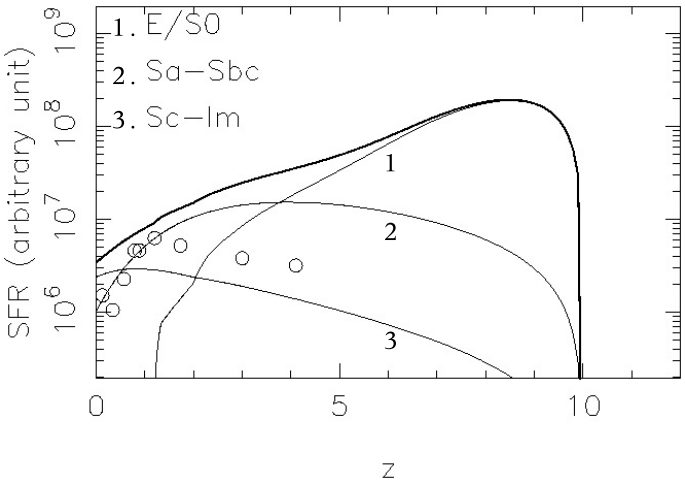

Fig. 9. Histories of the cosmic star-formation rate density (global and by types) derived from models of galaxy populations that fit optical and IR faint galaxy counts. The total $SFR(z)$ (heavy solid line) summed on all types is shown. The three $SFR_i(z)$ (thin lines) correspond to: 1) the major SFR at high reshifts ($z > 4$) is from E/SO galaxies, it induces the bulk of stars at early epochs 2) the intermediate SFR is from early spirals (Sa-Sbc), dominant from $z = 0.6$ to 4; it also fits the slope of the I-selected CFRS observations (empty circles), up to $z = 1$ before incompletness. 3) the weakest SFR is from Sc-Im galaxy types (late-type spirals and irregulars), dominant at $z \simeq 0$ where late galaxies are numerous and, still gas-rich, forming stars (see also Rocca-Volmerange 1999).

it is as low as 2 $M_\odot$ yr^{-1} for early 10^{11} $M_\odot$ spirals (Kennicutt 1983). This $SFR(t)$ variation is explained by the corresponding $M_{\rm gas}(t)$ variation. Because early spirals formed stars more efficiently in the past, their gas reservoir becomes depleted at $z \sim 1.5$, and the gas-dependent SFR then rapidly decreases from lack of fuel. This effect can explain the apparent "down-sizing" of galaxies (Panter et al. 2006).

When summing over all galaxy types, the total cosmic $SFR(z)$ increases at high redshift: it evolves by a factor $\leq$3 between $z = 0$ and 1. This result agrees with the gradual decline of the UV luminosity from the deep multi-wavelength Hawaiian surveys (Cowie et al. 1999) from $z = 1$ to $\simeq$0. This evolution is much less than the factor 10 decrease in the SFR derived from the shallower I-band selected CFRS sample (Lilly et al. 1996) on the same redshift range.The CFRS is an I-band selected sample, thus biased towards early spirals, the major emitters in the I band. This is confirmed by the good match between the $SFR(z)$ of the CFRS and that modelled for the Sa-Sbc galaxies in Fig. 9. We conclude that the I-band selection bias excludes late-type galaxies, too blue for detection in the I-band at the depth of CFRS. Models better agree with SFR estimates from Hα lines emitted by galaxies including a fraction of late types (Tresse et al. 2002).

8. Discussion

The faint galaxy counts at 12 μm in the *ISO*-ESS survey area show the same typical signature of evolution at 0.3 mJy as already found in the *ISO*/15 μm and *Spitzer*/24 μm galaxy counts. The careful flux calibration of the galaxy catalogue is based on the optical to mid-IR statistical properties of stars. Our results are consistent with the other mid-IR counts at 15 μm, thus demonstrating that the surveyed area of 680 arcmin square is sufficient for averaging the inhomogeneities and to properly analyse the populations of galaxies.

The most important result of our analysis is that a minor (<10%) population of dusty ultra-bright elliptical galaxies can explain the excess of the mid-IR emission observed in the 12 μm and 24 μm faint galaxy counts at $\simeq$0.3 mJy. Here, due to its high IR brightness, this population is associated to ULIRGs, while the other populations, seen in the UV-optical-nearIR and MIR counts, are called normal galaxies. Because the evolutionary code PÉGASE.3 predicts multi-wavelength SEDs by simultaneously following the evolution of stars, gas, dust and metal-enrichment, our analysis results find a natural explanation in the basic scenarios of galaxy evolution.

The strong advantage of our analysis is the multi-wavelength approach: the same SFR scenarios already found to fit the UV-optical-nearIR galaxy counts (Fioc & Rocca-Volmerange 1999a) are also applied to the MIR (12 μm, 15 μm, and 24 μm) using *ISO* (see companion article and Elbaz et al. 1999) and *Spitzer* satellites (Papovich et al. 2005; Le Floc'h et al. 2005). These evolutionary scenarios are robust because the evolution time scales of the dominant emitters at various wavelengths (massive stars, evolved stars, dust grains from the interstellar medium, and HII regions) go from a few million years to $\simeq$13 Gyr. In the mid-infrared, the new model with ULIRGs, proposed to fit *ISO*/12 μm galaxy counts is not likely to change the UV-optical-nearIR predictions; moreover it is confirmed by the *ISO*/15 μm and the more recent *Spitzer*/24 μm galaxy counts.

One difficulty of the interpretation is that, at $z \simeq 0$, the brightest Sbc spirals appear as luminous as dusty ultra-bright ellipticals in the MIR. Figures 5 to 8 show that the populations of "normal" ellipticals, spirals and irregulars (model 1) seen in the optical are largely insufficient for reproducing the 12 μm and 24 μm differential and cumulative counts. Even the brightest spirals (with $\log(L_*(12\,\mu{\rm m})/L_\odot) = 9.6$), which have IR luminosities comparable to ULIRGs at $z = 0$, decline too rapidly at increasing z to fit the 12 μm and 24 μm number counts.

A surprising result is that we succeed in reproducing the typical excess of MIR counts observed at $\simeq$0.3 mJy by only replacing 9% of the "normal" galaxies in the optical (and 1/3 of the ellipticals) with ultra-bright galaxies in the IR. In fact, at high redshift, the evolution correction takes over as the major parameter. It is noticeably insufficient for spirals while only ellipticals have high enough star formation rates for reproducing the stellar and dust emission at high redshifts. The fraction of these objects is small, and the enormous luminosities required can only be reached if these ULIRGs contain huge dust masses heated by large numbers of energetic photons.

The star formation history of ULIRGs follows that of elliptical galaxies shown in Fig. 9: large masses of stars and dust are formed at high z. ULIRGs would appear as "normal" ellipticals in the optical with masses of $\simeq 10^{12}$ $M_\odot$; they could even be more massive if the excess of stellar luminosity is hidden by a large amount of dust.

This dusty, massive population, revealed at high z in the mid-infrared, evokes the population of high-z (>4) massive ellipticals found in the K-z Hubble diagram (Rocca-Volmerange et al. 2004) and confirmed in the rest-frame H-z diagram with *Spitzer* (Seymour et al. 2007b): these distant galaxies are also forming high masses of stars and dust. Due to the short time scales required to build such objects at $z > 4$ (<1 Gyr), both populations most likely formed at early epochs by rapid dissipative collapse or major merging, rather than by slower hierarchical merging which would take $\simeq$10 Gyr.

This interpretation of ULIRGs as dusty massive ellipticals agrees with the drastic evolution of the infrared luminosity function when compared to the UV luminosity function (Takeuchi et al. 2006). It also agrees with the result that the MIR-selected galaxies contribute to more than 70% of the cosmic extragalactic background in the MIR (Dole et al. 2006): our model confirms that other galaxy types are too faint at both 12 μm and 24 μm. However, the conclusion of the last authors that galaxies contributing the most to the total cosmic infrared background have intermediate stellar masses is not confirmed by our results.

One puzzling issue is the over-brigthness of ellipticals in the mid-IR. It requires to know how the dust mass could be maintained within the galaxy host and the source of heating photons. To not be released by galactic winds, dust must not be mixed with gas and stars in the ISM but located in preferential zones such as the galaxy core. In the core, where the potential well becomes intense in case of an embedded black hole, dust could tend to be retained. In the AGN environment, the deep potential well would drag dust more efficiently, as it is more massive than gas, and dust then would fall more rapidly down into the inner core. Moreover if a Compton thick AGN is embedded within the proposed ULIRG/dusty ellipticals, the large variability from one ULIRG to another (Armus et al. 2006) is explained by orientation effects. Only observations at high spatial resolution will allow the dust geometry to be determined.

The other issue is the presence of a large number of energetic photons heating dust grains at all ages. To produce them, massive stars from an obscured starburst and/or the presence of an AGN can be evoked. Our results do not exclude that, in the case of galaxy interactions, an exceptionally extincted starburst, undetected in the optical, could be ultra-bright in the IR. But such an event is rare and is not representative of a galaxy population on a long time scale. Note that despite the high value of their MIR luminosity ($\log(L_*(12\ \mu\mathrm{m})/L_\odot) = 9.9$) at $z = 0$, the proposed ULIRGs faintly contribute to the faint UV-optical-NIR galaxy counts by their number. They also are suffering an exceptional extinction due to their dust amount. Further spectral syntheses and high spatial resolution are clearly needed. The recent analysis by Takeuchi et al. (2006), based on the combination of data from the UV satellite *GALEX* and from *IRAS*, shows that the luminosity function evolves more strongly in the far-infrared than in the far-UV. This is compatible with our dusty elliptical population. At last, by analysing the far-UV galaxy counts with FOCA at 2000 Å, Fioc & Rocca-Volmerange (1999a) suggested that a fraction of episodic starbursts could be required to interpret the UV excess of galaxy counts, in addition to the normal populations of galaxies. However, the number density, weak star formation rate, and low metallicity of these populations are not enough to explain the excess of MIR luminosity at high redshifts.

Finally, these scenarios of ultra-luminous galaxies at high redshifts, imply a very rapid phase of mass accumulation. This is also supported by the fact that ULIRGs, evolving as ellipticals and hosting a hidden AGN, look like the population of radio galaxies fitting the K-z diagram at high redshifts, which also show strong hot dust signatures (Rocca-Volmerange & Remazeilles 2005). However, the proposed population of distant ULIRGs derived from the infrared is more numerous (9%) than the radio-galaxy hosts detected in the optical (<4%). This indicates that half of the ULIRGs could be so obscured in the optical that they would be invisible. They may, however, be revealed at other wavelengths. Several surveys have discovered populations of AGN that appear brighter and spatially denser than the classical populations identified in the optical (see for example Martini et al. 2006). The population of hyper-LIRGs ($L_{\mathrm{IR}} > 10^{13}\ L_\odot$), sometimes associated to Ly α blobs, has a low $L_{\mathrm{Ly}\,\alpha}/L_{\mathrm{bol}}$ efficiency (0.05−0.2%) according to Colbert et al. (2005). The 12 μm and 24 μm galaxy counts analysed here may correspond to the best wavelength domain where this population of embedded AGNs could be detected.

9. Conclusion

We present the faint galaxy counts derived at 12 μm from the observation of a large and deep mid-infrared (MIR) survey in the field of the optical ESO-Sculptor Survey (ESS), through the large *LW10* filter with the ISOCAM instrument on board the *ISO* satellite. The infrared observations cover an area of ∼75% of the ESS spectroscopic survey, where galactic cirrus is sparse, and were performed in continuous raster mode. The flux calibration has been adjusted using optical-infrared IRAS colours ($B-12\,\mu$m, $V-12\,\mu$m) of standard stars. Because of its large area of ∼680 arcmin^2, the *ISO*-ESS survey provides complete 12 μm galaxy counts down to 0.24 mJy, after incompleteness corrections (using two independent methods). The full data analysis and the resulting catalogue of 142 detected sources is published in the companion paper, Seymour et al. (2007a).

The galaxy counts are presented using two different binnings: cumulative counts $N(>S)$, to reduce the fluctuations in the number density per bin, and Euclidean normalized differential counts $-S^{2.5}\mathrm{d}N/\mathrm{d}S$. When corrected for incompleteness, both the cumulative and differential *ISO*-ESS 12 μm counts averaged over the ∼680 arcmin^2 area show good agreement with the existing measurements in the nearby *ISOCAM* filter at 15 μm, after correction for the difference of wavelengths. In particular, the Euclidean-normalized differential counts of the *ISO*-ESS survey display the same excess as the other existing MIR surveys at flux densities of 0.3 mJy. This excess is also observed in the *Spitzer* galaxy counts at 24 μm.

We propose an interpretation of the cumulative and differential counts with the help of the new evolutionary code PÉGASE.3 (Fioc et al. 2007). For each galaxy type, PÉGASE.3 predicts the spectral energy distributions from the optical to the far-IR; the emission of stars and dust, the extinction, star formation history, metal enrichment, and dust mass are computed consistently.

With these evolutionary standard scenarios we have successfully modelled the multi-wavelength faint galaxy counts in the far-UV, optical, and near-infrared (Fioc & Rocca-Volmerange 1999a). In the present article, we are able to simultaneously fit the *ISO*-ESS 12 μm, *ISO* 15 μm and the *Spitzer*24 μm faint counts, by increasing the luminosity (≃2.5 mag at 12 μm to 5 mag at 24 μm) of a small fraction of galaxies (9%, all of elliptical type), while the rest of the galaxies (17.5% normal ellipticals, 57% spirals and 16.5% irregulars) are identical to the galaxy populations already known from the UV-optical-NIR surveys. The ultra-bright galaxies display all the characteristics of ULIRGs and appear as "normal" ellipticals in the optical. Because these results cover a very large wavelength domain, from the UV-optical-NIR to the MIR (12 μm, 15 μm, and 24 μm), we are confident the robustness of our scenarios.

The other important point is that no additional population of starbursts is required to fit the mid-IR excess. Highly luminous starbursts with a short e-folding time (≃10^7 years), which may explain some nearby ULIRGs such as M 82, are not incompatible with our results as long as they remain exceptional objects. Another point is that the normal galaxy populations, including bright IR spirals, cannot fit alone the cumulative or the differential *ISO*-ESS 12 μm and SPITZER 24 μm counts.

The star formation history of the proposed ULIRGs and normal ellipticals, in respective proportions of 1/3 and 2/3, can fully explain the excess in the cumulative and differential galaxy counts at 12 μm and 24 μm. A large dust mass and a large mass of early-formed stars as well as the possibility of an embedded Compton thick AGN could explain the ultra-brigthness of distant ULIRGs. The most distant ULIRGs would appear like the most massive ellipticals, similar to the distant radio galaxy hosts found in the K-z diagram (Rocca-Volmerange et al. 2004). As concluded in the mentioned article, this new result in the mid-IR favours the hypothesis of a galaxy evolution process based on dissipative collapse or a rapid merging on a short time scale (<1 Gyr) at high redshifts ($z > 5$).

We emphasise that these results are robust since they are derived from the simultaneous adjustment of the mid-IR 12 μm and 24 μm counts respecting the majority (>90%) of galaxies observed in the optical faint number counts (down to $B > 29$ from the HDF-N, William et al. 1996). Moreover, our analysis by type allows us to identify the various factors explaining the steep increase in the faint galaxy counts. Higher spectral and spatial resolution observations associated to deeper counts at longer wavelengths with the *Spitzer* satellite and the future *Herschel* satellite will hopefully allow detection of the dust emission emitted by early elliptical galaxies in their primitive epochs, validating our present results and allowing us to hopefully observe primeval galaxy populations down to the deepest extragalactic backgrounds.

Acknowledgements. N. Seymour acknowledges financial support from the European Network "Probing the Origin of the Extragactic Background Radiation" (POE) while at the Institut d'Astrophysique de Paris (IAP). We also thank Prof. L. Woltjer for his stimulating interest in this *ISO* observational program and Damien Le Borgne for his fruitful suggestions.

References

Altieri, B., Metcalfe, L., Kneib, J. P., et al. 1999, A&A, 343, 65
Arnouts, S., de Lapparent, V., Mathez, G., et al. 1997, A&AS, 124, 163
Aussel, H., Cesarsky, C. J., Elbaz, D., & Starck, J. L. 1999, A&A, 342, 313
Bellanger, C., de Lapparent, V., Arnouts, S., et al. 1995, A&AS, 110, 159
Bellanger, C., & de Lapparent, V. 1995, ApJ, 455, L103
Bertin, E., & Arnouts, S. 1996, A&AS, 117, 393
Cesarsky, C. J., Abergel, A., Agnese, P., et al. 1996, A&A, 315, 32
Caputi, K., Dole, H., Lagache, G., et al. 2006, ApJ, 637, 727
Chary, R.-R., Casertano, S., Dickinson, M. E., et al. 2004, ApJS, 154, 80
Chary, R.-R., Stern, D., & Eisenhardt, P. 2005, ApJ, 635, L5
Clements, D. L., Desert, F.-X., Franceschini, A., et al. 1999, A&A, 346, 383
Colbert, J. W., Teplitz, H. I., Yan, L., Malkan, M. A., & McCarthy, P. J. 2005, ApJ, 621, 587
Connolly, A. J., Szalay, A. S., Dickinson, M., Subbarao, M. U., & Brunner, R. J. 1997, ApJ, 486, L11
Couch, W. J., & Newell, E. B. 1980, PASP, 92, 746
Cowie, L. L., Songaila, A., & Barger, A. J. 1999, AJ, 118, 603
Dole, H., Lagache, G., Puget, J. L., et al. 2006, A&A, 451, 417
Draine, L. 2003, ARA&A, 41, 241
Egami, E., Dole, H., Huang, J.-S., et al. 2004, ApJS, 154, 130
Elbaz, D., Cesarsky, C. J., Fadda, D., et al. 1999, A&A, 351, L37
Fang, F., Shupe, D. L., Xu, C., & Hacking, P. B. 1998, ApJ, 500, 693
Fioc, M., & Rocca-Volmerange, B. 1997, A&A, 326, 950
Fioc, M., & Rocca-Volmerange, B. 1999a, A&A, 344, 393
Fioc, M., & Rocca-Volmerange, B. 1999b [arXiv:astro-ph/9912179]
Fioc, M., Rocca-Volmerange, B., & Dwek, E. 2007, A&A, near to submission
Flores, H., Hammer, F., Thuan, T. X., et al. 1999, ApJ, 517, 148
Galaz, G., & de Lapparent, V. 1998, A&A, 332, 459
Guhathakurta, P., & Draine, B. T. 1989, ApJ, 345, 230
Guiderdoni, B., & Rocca-Volmerange, B. 1990, A&A, 227, 362
Gruppioni, C., Pozzi, F., Lari, C., Oliver, S., & Rodighiero, G. 2005, ApJ, 618, L9
Hauser, M. G., Arendt, R. G., Kelsall, T., et al. 1998, ApJ, 508, 25
Heyl, J., Colless, M., Ellis, R. S., & Broadhurst, T. 1997, MNRAS, 285, 613
Hu, E. M., Cowie, L. L., McMahon, R. G., et al. 2002, ApJ, 568, L75
Kennicutt, R. C., Jr. 1983, ApJ, 272, 54
Kessler, M. F., Mueller, T. G., Leech, K., et al. 2003, ESASP, 1262
La Franca, F., Gruppioni, C., Matute, I., et al. 2004, AJ, 127, 3075
de Lapparent, V., & Slezak, E. 2007, A&A, submitted
de Lapparent, V., Galaz, G., Bardelli, S., & Arnouts, S. 2003, A&A, 404, 831
de Lapparent, V., Arnouts, S., Galaz, G., & Bardelli, S. 2004, A&A, 422, 841
de Lapparent, V., Seymour, N., & Rocca-Volmerange, B. 2007, in preparation
Le Borgne, D., & Rocca-Volmerange, B. 2002, A&A, 386, 446
Le Floc'h, E., Papovich, C., Dole, H., et al. 2005, ApJ, 632, 169
Lemonon, L., Pierre, M., Cesarsky, C. J., et al. 1998, A&A, 334, L21
Lilly, S. J., Le Fevre, O., Hammer, F., & Crampton, D. 1996, ApJ, 460, L1
Madau, P., Ferguson, H. C., Dickinson, M. E., et al. 1996, MNRAS, 283, 1388
Marleau, F. R., Fadda, D., Storrie-Lombardi, L. J., et al. 2004, ApJS, 154, 66
Martini, P., Kelson, D. D., Kim, E., Mulchaey, J. S., & Athey, A. A. 2006, ApJ, 644, 116
Moneti, A., & Breitfellner, M. G. 1997, Astrophys. Space Sci. Lib. Ser., 210, 205
Oliver, S. J., Goldschmidt, P., Franceschini, A., et al. 1997, MNRAS, 289, 471
Oliver, S., Rowan-Robinson, M., Alexander, D. M., et al. 2000, MNRAS, 316, 749
Oliver, S., Mann, R. G., Carballo, R., et al. 2002, MNRAS, 332, 536
Panter, B., Jimenez, R., Heavens, A. F., & Charlot, S. 2006 [arXiv:astro-ph/0608531]
Papovich, C., Dole, H., Egami, E., et al. 2004, ApJS, 154, 70
Pearson, C. 2005, MNRAS, 358, 1417
Pozzi, F., Ciliegi, P., Gruppioni, C., et al. 2003, MNRAS, 343, 1348
Pozzi, F., Gruppioni, C., Oliver, S., et al. 2004, ApJ, 609, 122
Press, W. H., & Schechter, P. 1974, ApJ, 187, 425
Puget, J.-L., & Leger, A. 1989, ARA&A, 27, 161
Puget, J.-L., Abergel, A., Bernard, J.-P., et al. 1996, A&A, 308, L5
Rana, N. C., & Basu, S. 1992, A&A, 265, 499
Rocca-Volmerange, B. 1999, in Toward a new millenium in galaxy morphology, ed. Block et al. (Kluwer), reprinted from Astrophysics and Space Science, 269, 238
Rocca-Volmerange, B., & Guiderdoni, B. 1988, A&AS, 75, 93
Rocca-Volmerange, B., & Remazeilles, M. 2005, A&A, 433, 73
Rocca-Volmerange, B., Le Borgne, D., De Breuck, C., Fioc, M., & Moy, E. 2004, A&A, 415, 931
Rodighiero, G., Lari, C., Fadda, D., et al. 2004, A&A, 427, 773
Rodighiero, G., Lari, C., Pozzi, P., et al. 2006, MNRAS, 371, 1891
Rowan-Robinson, M., Oliver, S., Efstathiou, A., et al. 1999, in The Universe as Seen by *ISO*, ed. P. Cox, & M. F. Kessler, ESA-SP, 427, 1011
Rowan-Robinson, M., Lari, C., Perez-Fournon, I., et al. 2004, MNRAS, 351, 1290
Rush, B., Malkan, M. A., & Spinoglio, L. 1993, ApJS, 89, 1
Sato, Y., Kawara, K., Cowie, L. L., et al. 2003, A&A, 405, 833
Serjeant, S., Oliver, S., Rowan-Robinson, M., et al. 2000, MNRAS, 317, 29
Seymour, N., Rocca-Volmerange, B., & de Lapparent, V. 2007a, A&A, 475, 791
Seymour, N., Stern, D., De Breuck, C., et al. 2007b, ApJS, 171, 353
Shupe, D. L., Fang, F., Hacking, P. B., & Huchra, J. P. 1998, ApJ, 501, 597
Silva, L., Granato, G. L., Bressan, A., & Danese, L. 1998, ApJ, 509, 103
Soifer, B. T., Helou, G., Lonsdale, C., et al. 1984, ApJ, 283, L1
Somerville, R. S., Lee, K., Ferguson, H. C., et al. 2004, ApJ, 600, L171
Spergel, D. N., Verde, L., Peiris, H. V., et al. 2003, ApJS, 148, 175
Starck, J. L., Abergel, A., Aussel, H., et al. 1999, A&AS, 134, 135
Takeuchi, T. T., Buat, V., & Burgarella, D. 2006 [arXiv:astro-ph/0611796]
Taniguchi, Y., Cowie, L. L., Sato, Y., et al. 1997, A&A, 328, 9
Tresse, L., Maddox, S. J., Le Fèvre, O., & Cuby, J. G. 2002, MNRAS, 337, 369
Verstraete, L., Pech, C., Moutou, C., et al. 2000, The 2nd *ISO* workshop on analytical spectroscopy, ed. A. Salama, M. F. Kessler, K. Leech, & B. Schulz, ESA-SP, 456, 319
Werner, M. W., Roellig, T. L., Low, F. J., et al. 2004, ApJS, 154, 1
Weinberg, S. 1972, Gravitation and cosmology: Principles and applications of the general theory of relativity (New York: Wileys)
Williams, R. E., Blacker, B., Dickinson, M., et al. 1996, AJ, 112, 1335
Xilouris, E. M., Madden, S. C., Galliano, F., Vigroux, L., & Sauvage, M. 2004, A&A, 416, 41